ACS Partner Journal
PRECISION CHEMISTRY
pubs.acs.org/PrecisionChem

Article

Substrate-Induced Interfacial Coupling between Graphene and Copper

Chong Zhao,*,# Qianyi Liu,# Zhibin Zhang,# Mengze Zhao, Qingqiu Cheng, Yue Zhao, Muhong Wu,* and Kaihui Liu*

Cite This: https://doi.org/10.1021/prechem.6c00002

ABSTRACT: Graphene/copper (Gr/Cu) composites, which combine the exceptional electrical, thermal, and mechanical properties of both components, have emerged as a promising platform for advanced electronic and energy storage applications. Successful studies have been done on optimizing graphene incorporation and morphology, while the impact of Gr/Cu interfacial interactions on composite performance remains underexplored. Here, we systematically investigate eight Gr/Cu interfaces and clarify their interfacial coupling relationships. Our results demonstrate that the doping level of graphene closely correlates with the crystallographic orientation of Cu, where Gr/Cu(111) exhibits the highest electron doping level, and Gr/Cu(332) shows the lowest. Higher doping is accompanied by greater graphene surface friction, revealing a direct link between charge transfer at the interface and tribological behavior. Crystallographic orientation control represents an atomically precise interfacial engineering strategy for tailoring interfacial coupling. Through this approach, charge transfer and friction can be effectively tuned, paving the way for the rational design of high-performance Gr/Cu composites for applications such as efficient power transmission, reliable electrical interconnects, and low-friction systems.

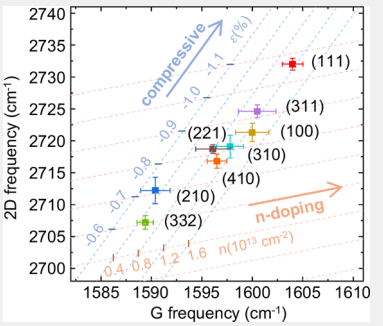

KEYWORDS: *graphene, copper, composites, interfacial coupling, friction*

INTRODUCTION

The pursuit of next-generation functional materials has brought Gr/Cu composites to the forefront of advanced materials research, due to their exceptional combination of ultrahigh electrical conductivity,[1] outstanding thermal stability,[2] and superior mechanical durability.[3] These remarkable properties originate from the unique ability of graphene to modulate charge transport pathways at metal interfaces while preserving the intrinsic characteristics of Cu. In the past two decades, extensive efforts have focused on improving graphene quality[4,5] and optimizing composite architectures,[6−8] which have significantly enhanced the overall performance of Gr/Cu systems. Meanwhile, interfacial coupling, defined as the atomic-level interaction between graphene and Cu, has also been identified as a key factor influencing the composite properties.[9,10]

In essence, the macroscopic properties of Gr/Cu composites arise from the collective behavior of individual graphene, Cu, and their interfacial junctions. Given the well-established intrinsic properties of both graphene and Cu, the interfacial region emerges as the decisive factor controlling the overall performance of the composites. Fundamentally, the nature of the Gr/Cu interface can be affected by several factors, including structural defects, impurity adsorption, and the crystallographic orientation of the Cu surface. Under optimized graphene growth conditions where extrinsic adsorbates are minimized, the crystallographic orientation of the Cu substrate becomes the predominant factor modulating the interfacial behavior through variations in atomic coordination.[11,12]

Despite the well-recognized importance of Cu crystallographic orientation in governing the performance of Gr/Cu composites, most existing studies have centered on polycrystalline Cu or low-index facets. Among them, the Cu(111) surface has been most studied, primarily due to the substantial fabrication challenges of other high-index facets (arising from their thermodynamically and kinetically unfavorable characteristics).[13] This preference has significantly advanced the research of Gr/Cu(111)-based systems in promoting their performance, while leaving other Cu facets comparatively underexplored. As a result, the fundamental relationship between surface atomic structure and interfacial coupling mechanisms—including charge transfer and strain coupling—remains insufficiently understood. A more comprehensive mechanistic understanding of orientation-dependent interfacial behavior, especially the quantitative mapping of interfacial coupling across Gr/Cu(hkl) interfaces, is essential for tailoring

Received: January 4, 2026
Revised: March 4, 2026
Accepted: March 5, 2026

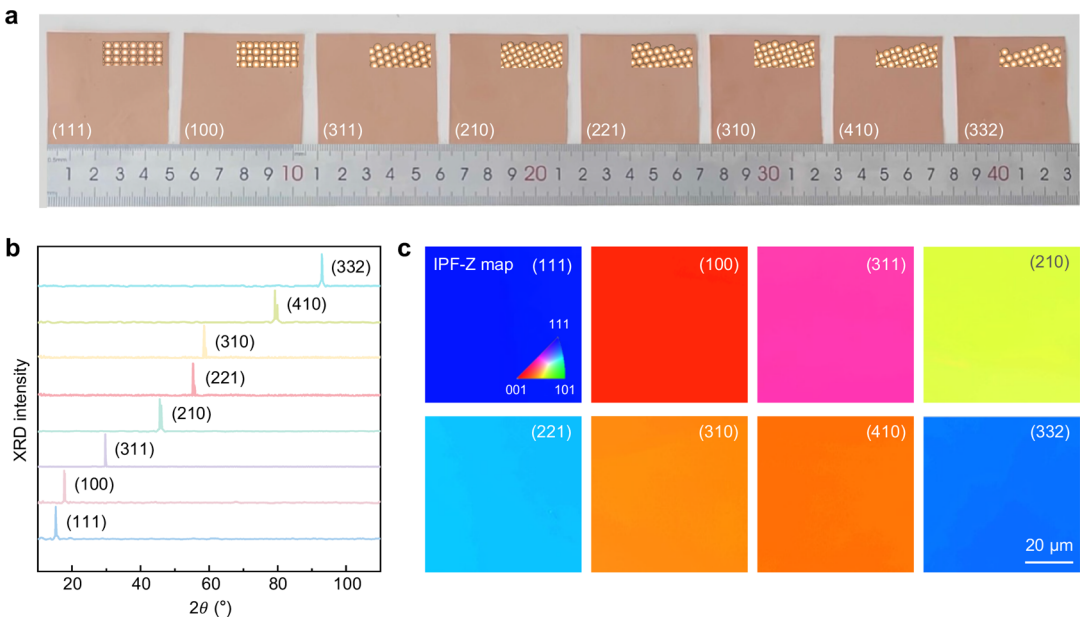

Figure 1. Photographs and orientation characterization of single-crystal Cu(hkl) foils. (a) Optical image of the eight representative single-crystal Cu(*hkl*) foils with a typical size of 5 × 5 cm^2. The inset in the upper right corner illustrates the side-view atomic arrangements corresponding to each crystallographic surface. (b, c) XRD 2θ scan spectra (b) and EBSD IPF-Z maps (c) of the eight kinds of single-crystal Cu foil.

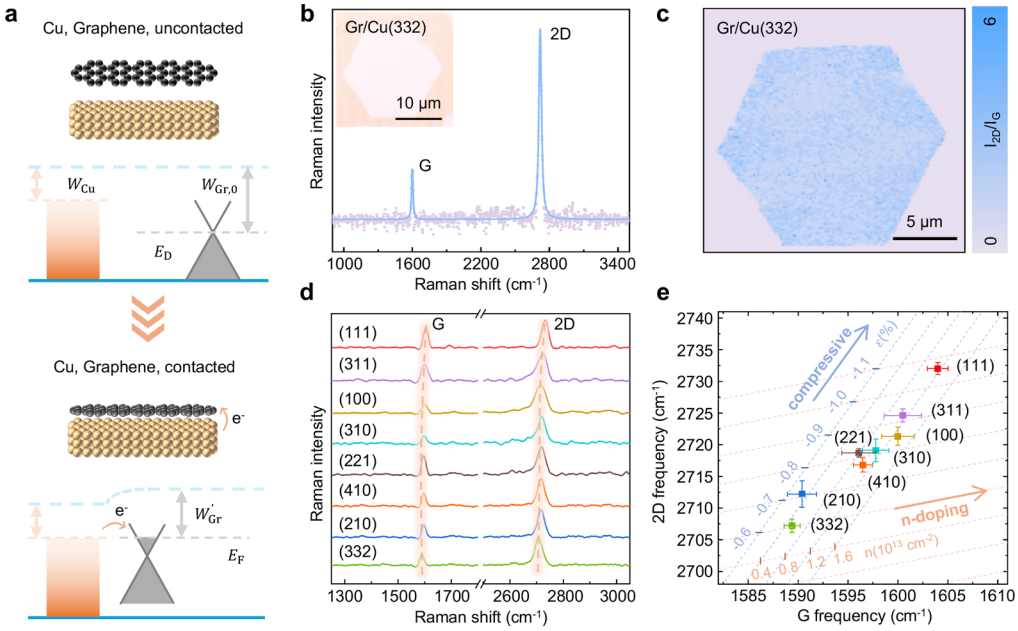

Figure 2. Doping analysis of Gr/Cu(hkl) samples. (a) Schematic illustration of the energy level alignment between graphene and the Cu substrate before and after contact. (b) Raman spectrum of monolayer graphene grown on Cu(332). Inset: Optical image of monolayer graphene on Cu(332). (c) Corresponding Raman mapping of the I_{2D}/I_G ratio for graphene in (b). (d) Raman spectra of monolayer graphene grown on eight different Cu(hkl) foils. (e) Correlation between the G peak (ω_G) and 2D peak (ω_{2D}) frequencies in the Raman spectra of graphene on eight Cu(hkl) foils.

graphene's electronic properties and guiding the rational design of Gr/Cu-based functional materials.

In this study, we synthesized high-quality graphene on eight well-defined single-crystal Cu substrates, enabling a systematic investigation on how crystallographic orientation regulates the interfacial coupling at Gr/Cu(hkl) junctions. High-resolution structural and spectroscopic characterization techniques were employed to enable the distinction of electron doping levels, surface potentials, and frictional behavior across different Cu facets. This comprehensive data set reveals orientation-dependent trends in interfacial electronic characteristics and frictional responses, thereby establishing a direct correlation between substrate crystallography and functional interfacial properties.

RESULTS AND DISCUSSION

In our experiment, Cu foils with various facets were synthesized using the developed seeded-growth method.[14] Specifically, a mild preoxidation treatment was utilized to create a Cu_xO/Cu interface that transformed the driving force

https://doi.org/10.1021/prechem.6c00002
Precis. Chem. XXXX, XXX, XXX−XXX

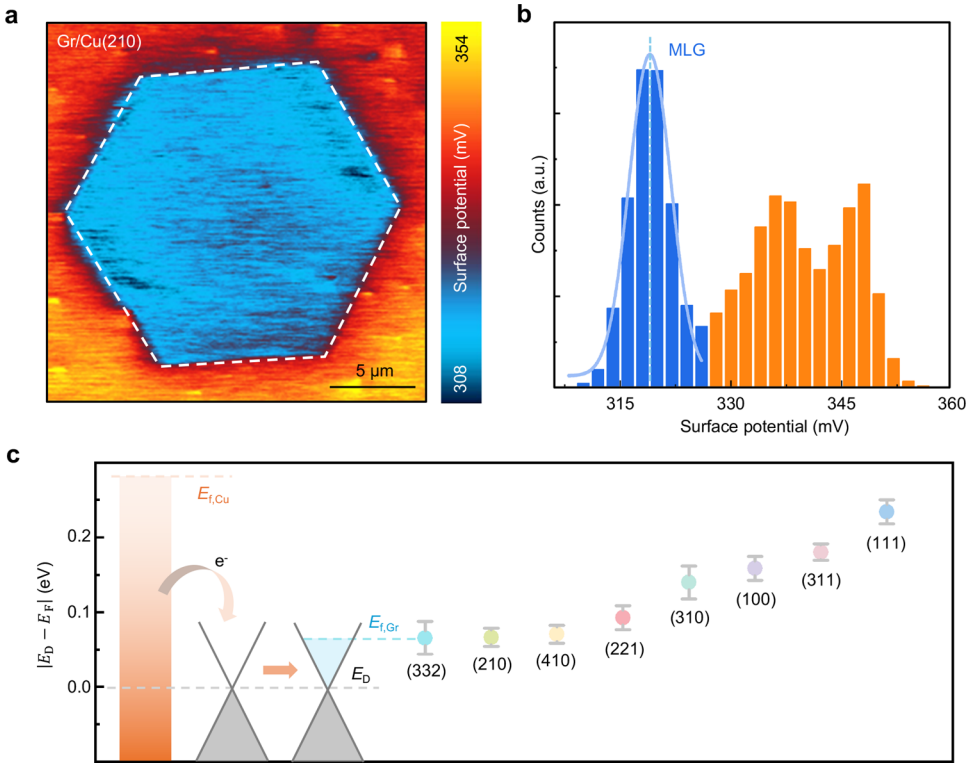

Figure 3. Surface potential analysis of Gr/Cu(hkl) samples. (a) Surface potential distribution of monolayer graphene on Cu(210). (b) Histogram of the surface potential in (a). (c) Calculated Fermi level shift of monolayer graphene on eight different Cu(hkl) foils.

for grain growth from surface energy to interface energy, promoting the nucleation and growth of high-index Cu(hkl) seeds. This approach enabled the successful synthesis of eight types of single-crystal Cu(hkl) foils (5 cm × 5 cm, Figures 1a and S1 in the Supporting Information) with superior crystallographic quality. The facet indices were identified through X-ray diffraction (XRD) with characteristic 2θ peaks (Figure 1b, with a silver target). The uniformity of the single crystals was further confirmed by electron backscatter diffraction (EBSD) inverse pole figure (IPF-Z) mappings with consistent color regions (Figures 1c and S2 in the Supporting Information).

Using these high-quality single-crystal Cu foils, graphene was subsequently synthesized following the standard growth procedure (see Experimental Details). Then, a systematic investigation of interfacial coupling in the composite systems was readily conducted. Given the difference in work function between graphene and Cu, van der Waals contact at the interface would induce charge transfer to equilibrate their Fermi levels (Figure 2a). As Raman is highly sensitive to the doping-induced vibrational shifts in graphene, it was thus employed as a primary tool to probe the variations in carrier concentration across the Gr/Cu(hkl) samples.

First, Raman was utilized to evaluate the quality of the grown graphene. Both single-point spectra and Raman mapping confirmed the high structural quality and uniformity of the synthesized graphene across all Cu(hkl) surfaces. The absence of a defect-related D peak near 1350 cm^{-1} (Figure 2b, Gr/Cu(332) as an example) indicates that the synthesized graphene is free of structural defects.[15] Furthermore, Raman intensity mapping of the 2D-to-G peak ratio (I_{2D}/I_G) exhibited excellent spatial uniformity (Figure 2c), suggesting that the graphene coverage is highly homogeneous, with no apparent multilayer regions. These spectroscopic features provide a reliable foundation for subsequent analysis of orientation-dependent doping behaviors.

Subsequently, we analyzed the Raman spectra of graphene to investigate the interfacial charge transfer behavior. In particular, systematic shifts in the G-band position (ω_G) provided direct evidence of crystallographic orientation-dependent doping behavior.[16] Our experimental results revealed that the G-band position exhibited a gradual blueshift from Cu(332) to Cu(111), following the sequence of Cu(332), Cu(210), Cu(410), Cu(221), Cu(310), Cu(100), Cu(311), and Cu(111) (Figure 2d). This blueshift reflects stronger electron−phonon coupling, which is caused by increased carrier doping and enhanced interfacial interaction.[17−19] Naturally, doping in graphene arises from interfacial charge transfer, which typically proceeds from the material with the lower work function to the one with the higher work function. In the case of Gr/Cu contacts, the situation is modified by the formation of an interfacial potential step ($\Delta_c \sim$ 0.9 eV for Cu(111)), resulting from charge redistribution at the Gr/Cu interface.[20,21] This charge rearrangement creates an interfacial dipole that effectively lowers the local vacuum level on the Cu side, altering the apparent work function alignment between the two materials. As a result, the relative work functions follow a well-defined hierarchy: $W_{Cu(hkl)} < W_{Gr,0} < W_{Cu(111)} < W_{Gr,0} + \Delta_c$, where $W_{Cu(hkl)}$, $W_{Gr,0}$, and $W_{Cu(111)}$ are the work functions of Cu(hkl), intrinsic graphene, and Cu(111), respectively, and $W_{Gr,0}$ is about 4.67 ± 0.11 eV. This ordering is consistent with both theoretical calculations and experimental measurements.[22−24] Such an energy alignment favors electron transfer from Cu to graphene, resulting in intrinsic n-type doping across all Cu surface orientations considered.[25]

https://doi.org/10.1021/prechem.6c00002
Precis. Chem. XXXX, XXX, XXX−XXX

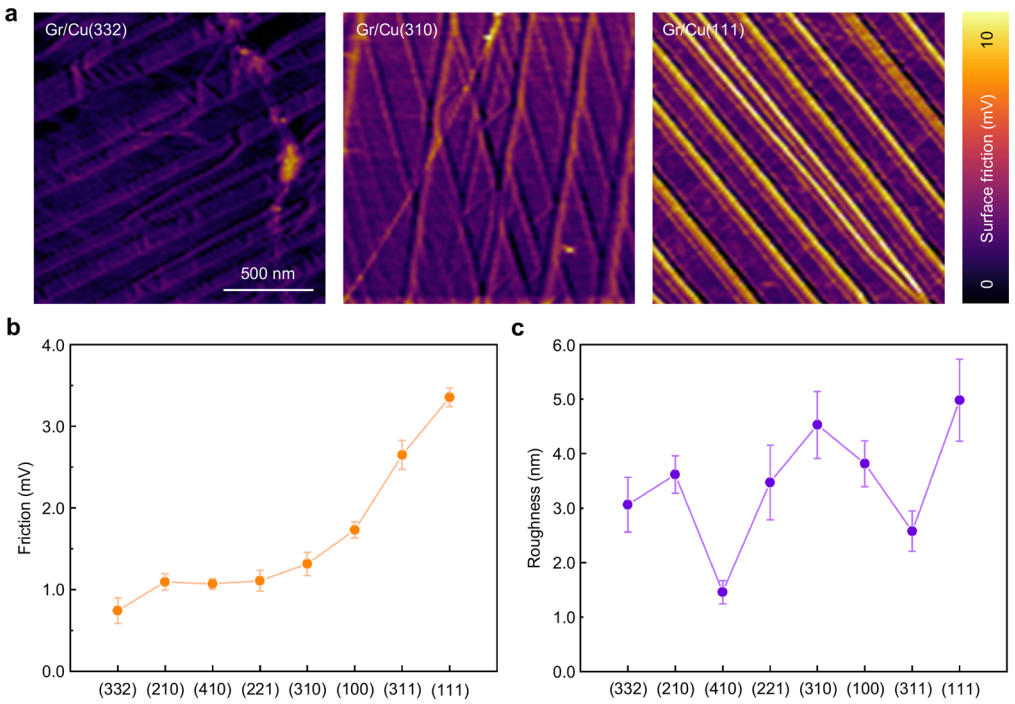

Figure 4. Friction analysis of Gr/Cu(hkl) samples. (a) Friction force images of the Cu(332), Cu(310), and Cu(111) foils covered by monolayer graphene. (b, c) Statistical analysis of friction forces (b) and surface roughness (c) of monolayer graphene on eight Cu(hkl) foils.

To quantitatively evaluate the doping concentrations, we further employed the optical separation method to analyze the correlation between ω_{2D} and ω_G shifts.[26] In the ω_G–ω_{2D} scatter plot (Figure 2e), the blue dashed line ($\Delta\omega_{2D}/\Delta\omega_G$ = 2.2) represents strain effects under constant doping, while the pink dashed line ($\Delta\omega_{2D}/\Delta\omega_G$ = 0.3) denotes n-type doping effects under constant strain. By performing vector decomposition relative to the Raman peak positions of suspended monolayer graphene (on silicon substrates with 5 μm holes, ω_G = 1572 cm^{-1}, ω_{2D} = 2675 cm^{-1}; see Figure S3 in the Supporting Information),[27] we quantitatively extracted both carrier concentrations and strain levels in graphene on different Cu(hkl) substrates from the ω_{2D} and ω_G shifts (Figure 2e). Model analysis indicates that Gr/Cu(111) exhibits a carrier concentration of ~1.2 × 10^{13} cm^{-2} with a compressive strain of ~1.06%, whereas Gr/Cu(210) shows a lower carrier concentration of ~0.3 × 10^{13} cm^{-2} and a compressive strain of ~0.71%. These results confirm that crystallographic orientation exerts a substantial influence on graphene/metal interfacial charge transfer.

Notably, both strain and charge transfer exhibit the same crystallographic dependence, suggesting that they arise from a common origin, which is the interfacial coupling between graphene and Cu(hkl). Stronger interfacial coupling enhances electron transfer to graphene, while simultaneously restricting its relaxation during postgrowth cooling, thereby resulting in larger compressive strain.[28,29] These results confirm that crystallographic orientation systematically modulates interfacial coupling strength, and that strain and doping serve as two important signatures of this interaction.

Furthermore, to obtain a more direct determination of the interfacial couplings, we conducted Kelvin Probe Force Microscopy (KPFM) measurements by measuring the surface potential distribution. In our experiments, we focused on comparing the doping effects of different Cu(hkl) substrates by analyzing variations in graphene's Fermi level. In principle, the energy offset between the Fermi level (E_F) and the Dirac point (E_D) of graphene is proportional to the square root of the carrier concentration ($|E_D - E_F| \propto \sqrt{n}$).[30] And such energy offset can be obtained from the measured work function (W'_{Gr}) using Equation 1:[31]

$$|E_D - E_F| = W'_{Gr} - W_{Gr,0} \quad (1)$$

The work function of graphene could be extracted from KPFM surface potential maps (Figures 3a and S4 in the Supporting Information), where graphene (blue) and Cu substrate regions (orange) are clearly distinguished. Although KPFM inherently measures relative surface potentials, the combination of statistical analysis and Gaussian fitting enables a more accurate determination of the surface potentials of both graphene and the underlying Cu(hkl) substrates.

By measuring the surface potential difference between graphene and the Highly Oriented Pyrolytic Graphite (HOPG) reference sample, we directly quantified the relative doping concentrations of graphene on different Cu(hkl) substrates (Figure 3c and Section S1 in the Supporting Information). Given the known work function difference (W'_{Gr} – $W_{Gr,0}$), the Fermi level shift $|E_D - E_F|$ can be extracted. Larger $|E_D - E_F|$ values indicate higher electron doping levels, and the observed doping trends of graphene across the eight Cu(hkl) facets were consistent with the results obtained from Raman analysis (Figure 3c). Moreover, local variations in surface potential (such as subtle color differences in the potential maps) were also detected, which may originate from the inherent roughness of the Cu(hkl) surfaces and the graphene wrinkles.[32] From a statistical perspective, these minor variations do not significantly affect the overall average surface potential.

Through our detailed investigations, a systematic relationship between graphene's doping level and the orientation of Cu substrates was established (Table S1 in the Supporting

https://doi.org/10.1021/prechem.6c00002
Precis. Chem. XXXX, XXX, XXX−XXX

Information). The measured doping levels follow the descending order: Cu(111) > Cu(311) > Cu(100) > Cu(310) > Cu(221) > Cu(410) > Cu(210) > Cu(332). Among these, Cu(111) exhibits the highest atomic packing density and the closest lattice matching with graphene, resulting in the strongest coupling strength and the highest n-type doping concentration.[33,34] In contrast, high-index surfaces such as Cu(332) exhibit pronounced atomic step−terrace structures (Figure S1 in the Supporting Information), which weakens effective interfacial coupling and results in reduced charge transfer. This experimental trend aligns well with theoretical predictions of coupling strength: the calculated close contact index, derived from the atomic configurations of Cu(hkl) surfaces, peaks at Cu(111) and reaches a minimum at Cu(332). These results collectively indicate that the interfacial electron doping exhibits a strong correlation with coupling strength.[35,36]

Stronger interfacial coupling is expected to exert a greater influence on the mechanical behavior of layered materials.[37] In the case of Gr/Cu(hkl) composites, such enhanced coupling—associated with higher doping concentrations—is expected to lead to increased surface friction. Here, we characterized the surface morphology and roughness using atomic force microscopy (AFM) in tapping mode, while friction force measurements (FFM) were also performed at the same positions to quantify friction on the graphene surface. The AFM imaging revealed that the morphology of graphene is influenced by the underlying Cu substrate, with graphene partially replicating the stepped features of the Cu(hkl) surfaces (Figures 4a and S5 in the Supporting Information).[38−40] FFM further showed that the surface friction of graphene increases with electron doping across the eight Gr/Cu(hkl) samples (Figure 4b), highlighting a strong correlation between charge transfer and tribological behavior.

In contrast, no clear correlation was observed between surface roughness and friction (Figure 4c), that is, samples exhibiting higher friction did not necessarily possess higher surface roughness. These results suggest that interfacial electronic coupling, rather than topographic features alone, plays a critical role in modulating graphene's frictional response. From a materials design and processing standpoint, these results indicate that the choice of Cu crystallographic orientation provides a practical route to pre-engineer interfacial friction at the graphene/metal interface. Cu substrates with weaker interfacial coupling (e.g., high-index facets) are expected to minimize interfacial frictional dissipation during graphene growth and integration processes, whereas strongly coupled surfaces (e.g., Cu(111)) may be advantageous where enhanced interfacial adhesion or mechanical robustness of the as-grown graphene/metal interface is required. Such findings provide new insights into the interplay between electronic structure and nanoscale friction, thereby expanding the conventional understanding that primarily links friction to surface topography.[41]

CONCLUSIONS

In conclusion, this study demonstrates that the crystallographic orientation of Cu substrates significantly influences interfacial coupling with graphene, thereby regulating both the n-type carrier concentration and surface friction of graphene. Both doping level and friction of Gr/Cu(*hkl*) samples follow a consistent trend across the studied orientations: Cu(111) > Cu(311) > Cu(100) > Cu(310) > Cu(221) > Cu(410) > Cu(210) > Cu(332). These findings offer fundamental insight into interfacial charge transfer mechanisms and establish substrate-induced interfacial coupling as a key parameter for tailoring the electronic and tribological properties of graphene/metal composites. More broadly, crystallographic orientation is identified as an atomically defined parameter for tuning interfacial couplings, providing a strategy for engineering charge transfer and friction in other 2D material/metal systems.

EXPERIMENTAL DETAILS

Synthesis of Single-Crystal Cu Foils

Polycrystalline Cu foil (25 μm thick, 99.8%; Zhongke Jingyi (Dongguan) Materials Technology Co., Ltd.) was mounted on a quartz substrate and loaded into a hot-wall tube furnace (Tianjin Kaiheng Co., Ltd.). The sample was heated to 160−200 °C in ambient air and maintained at this temperature for 1−2 h to promote surface oxidation. The preoxidation treatment was carried out under laboratory ambient conditions (relative humidity of 22%), with all samples processed under identical conditions. Subsequently, the preoxidized Cu foil was annealed at 1040 °C under a reducing atmosphere composed of 500 standard cubic centimeters per minute (sccm) Ar and 50 sccm H_2 for 3−5 h. The furnace was then allowed to cool naturally to room temperature, yielding single-crystal Cu(hkl) foils.

Synthesis of Graphene

The Cu(*hkl*) foil was transferred onto a quartz substrate and placed in a chemical vapor deposition furnace (Tianjin Kaiheng Co., Ltd.). The system was heated to 1040−1050 °C under a reducing atmosphere of 500 sccm Ar and 10 sccm H_2. Graphene growth was initiated by introducing 0.05 sccm CH_4 along with 50 sccm H_2 into the reaction zone for 20 min. After growth, the sample was cooled naturally under the same reducing conditions, resulting in hexagonal graphene domains on the Cu(*hkl*) surface.

Characterization

X-ray diffraction (XRD, 2θ scans) was performed using a Bruker D8 Advance system equipped with a silver target ($\lambda \approx 0.56$ Å), optimized for Cu(*hkl*) analysis. Electron backscatter diffraction (EBSD) was conducted using a Verios 5UC field-emission scanning electron microscope (FE-SEM). Raman spectra were collected with a WITec alpha300 R system using a 514 nm excitation laser. Atomic force microscopy (AFM) and Kelvin probe force microscopy (KPFM) measurements were carried out using a Cypher S system (Oxford Instruments). All friction force measurements were performed at a fixed scan angle of 90° under identical imaging and scanning conditions. All Raman, KPFM, and FFM measurements were performed directly on samples without transfer, in a cleanroom environment at a temperature of 25 °C and a relative humidity of 22%. All measurements were completed within 60 min after the sample preparation.

ASSOCIATED CONTENT

Data Availability Statement

The data that support the findings of this study are available within the paper and Supporting Information. Additional data are available from the corresponding authors upon request.

Supporting Information

The Supporting Information is available free of charge at https://pubs.acs.org/doi/10.1021/prechem.6c00002.

Additional details on the experimental methodology and extended characterization results, including work function calibration, atomic structures of Cu(*hkl*) surfaces, EBSD orientation mapping, AFM and Raman characterization of suspended graphene, KPFM surface

https://doi.org/10.1021/prechem.6c00002
Precis. Chem. XXXX, XXX, XXX−XXX

potential measurements, and friction performance analysis (PDF)

AUTHOR INFORMATION

Corresponding Authors

Chong Zhao − *Songshan Lake Materials Laboratory, Institute of Physics, Chinese Academy of Sciences, Dongguan 523000, China*; orcid.org/0009-0001-9406-5598; Email: zhaochong@sslab.org.cn

Muhong Wu − *Songshan Lake Materials Laboratory, Institute of Physics, Chinese Academy of Sciences, Dongguan 523000, China; Institute of Atomic Manufacturing, International Institute for Interdisciplinary and Frontiers, Beihang University, Beijing 100191, China; Interdisciplinary Institute of Light-Element Quantum Materials and Research Center for Light-Element Advanced Materials, Peking University, Beijing 100871, China*; Email: muhongwu@buaa.edu.cn

Kaihui Liu − *Songshan Lake Materials Laboratory, Institute of Physics, Chinese Academy of Sciences, Dongguan 523000, China; State Key Laboratory for Mesoscopic Physics, Frontiers Science Center for Nano-optoelectronics, School of Physics, Peking University, Beijing 100871, China*; orcid.org/0000-0002-8781-2495; Email: khliu@pku.edu.cn

Authors

Qianyi Liu − *Songshan Lake Materials Laboratory, Institute of Physics, Chinese Academy of Sciences, Dongguan 523000, China*

Zhibin Zhang − *State Key Laboratory for Mesoscopic Physics, Frontiers Science Center for Nano-optoelectronics, School of Physics, Peking University, Beijing 100871, China*

Mengze Zhao − *State Key Laboratory for Mesoscopic Physics, Frontiers Science Center for Nano-optoelectronics, School of Physics, Peking University, Beijing 100871, China*

Qingqiu Cheng − *Songshan Lake Materials Laboratory, Institute of Physics, Chinese Academy of Sciences, Dongguan 523000, China*

Yue Zhao − *Guangdong Provincial Key Laboratory of Advanced Thermoelectric Materials and Device Physics and Department of Physics and Guangdong Basic Research Center of Excellence for Quantum Science, Southern University of Science and Technology, Shenzhen 518055, China*; orcid.org/0000-0002-9174-0519

Complete contact information is available at: https://pubs.acs.org/10.1021/prechem.6c00002

Author Contributions

#C.Z., Q.L., Z.Z. contributed equally to this work.

Funding

This work was supported by the Guangdong Major Project of Basic and Applied Basic Research (2021B0301030002 (K.L.)), the National Natural Science Foundation of China (92577201 (K.L.), 52172035 (M.W.), 52402043 (Z.Z.), U25A20483 (M.W.), and U24A20285 (Z.Z.)), the National Key R&D Program of China (2021YFA1400502 (M.W.)), and the New Cornerstone Science Foundation through the XPLORER PRIZE (K.L.).

Notes

The authors declare no competing financial interest.

REFERENCES

(1) Cao, M.; Xiong, D. B.; Yang, L.; Li, S.; Xie, Y.; Guo, Q.; Li, Z.; Adams, H.; Gu, J.; Fan, T.; et al. Ultrahigh Electrical Conductivity of Graphene Embedded in Metals. *Adv. Funct. Mater.* **2019**, *29* (17), No. 1806792.

(2) Zhao, M.; Zhang, Z.; Shi, W.; Li, Y.; Xue, C.; Hu, Y.; Ding, M.; Zhang, Z.; Liu, Z.; Fu, Y.; et al. Enhanced copper anticorrosion from Janus-doped bilayer graphene. *Nat. Commun.* **2023**, *14* (1), 7447.

(3) Kim, Y.; Lee, J.; Yeom, M. S.; Shin, J. W.; Kim, H.; Cui, Y.; Kysar, J. W.; Hone, J.; Jung, Y.; Jeon, S.; Han, S. M. Strengthening effect of single-atomic-layer graphene in metal−graphene nanolayered composites. *Nat. Commun.* **2013**, *4* (1), 2114.

(4) Gao, Z.; Zuo, T.; Wang, M.; Zhang, L.; Da, B.; Ru, Y.; Xue, J.; Wu, Y.; Han, L.; Xiao, L. In-situ graphene enhanced copper wire: A novel electrical material with simultaneously high electrical conductivity and high strength. *Carbon* **2022**, *186*, 303−312.

(5) Wang, Y.; Zhong, B.; Ni, J.; Song, J.; Huang, Y.; Yao, S.; Liu, Y.; Fan, T. Enhanced electrical conductivity of copper by nitrogen-doped graphene. *Scripta Materialia* **2024**, *239*, No. 115797.

(6) Li, T.; Wang, Y.; Yang, M.; Hou, H.; Wu, S. High strength and conductivity copper matrix composites reinforced by in-situ graphene through severe plastic deformation processes. *J. Alloys Compd.* **2021**, *851*, No. 156703.

(7) Shu, S.; Yuan, Q.; Dai, W.; Wu, M.; Dai, D.; Yang, K.; Wang, B.; Lin, C.-T.; Wuebben, T.; Degenhardt, J.; et al. In-situ synthesis of graphene-like carbon encapsulated copper particles for reinforcing copper matrix composites. *Mater. Des.* **2021**, *203*, No. 109586.

(8) Jiang, B.; Liu, C.; Dai, B.; Pei, Z.; Liu, B.; Wang, Y. Improved strength-plasticity-conductivity of graphene/copper layered composites by vacuum hot rolling. *Journal of Materials Research and Technology* **2024**, *31*, 1991−2002.

(9) Liu, Y.; Zhang, J.; Niu, R.; Bayat, M.; Zhou, Y.; Yin, Y.; Tan, Q.; Liu, S.; Hattel, J. H.; Li, M.; et al. Manufacturing of high strength and high conductivity copper with laser powder bed fusion. *Nat. Commun.* **2024**, *15* (1), 1283.

(10) Yang, K. M.; Li, Q.; Zhang, Q.; Liu, G. S.; Wang, J. J.; Yang, Y. F.; Guo, C. X.; Ni, J. M.; Song, J.; Zhang, J.; et al. Synergistically enhanced interface stability by graphene assisted copper surface reconstruction. *Acta Mater.* **2022**, *226*, No. 117638.

(11) Liu, X.; Zhang, J.; Wang, W.; Zhao, W.; Chen, H.; Liu, B.; Zhang, M.; Liang, F.; Zhang, L.; Zhang, R.; et al. The role of Cu crystallographic orientations towards growing superclean graphene on meter-sized scale. *Nano Research* **2022**, *15* (4), 3775−3780.

(12) Li, X.; Wu, G.; Zhang, L.; Huang, D.; Li, Y.; Zhang, R.; Li, M.; Zhu, L.; Guo, J.; Huang, T.; et al. Single-crystal two-dimensional material epitaxy on tailored non-single-crystal substrates. *Nat. Commun.* **2022**, *13* (1), 1773.

(13) Nguyen, V. L.; Duong, D. L.; Lee, S. H.; Avila, J.; Han, G.; Kim, Y.-M.; Asensio, M. C.; Jeong, S.-Y.; Lee, Y. H. Layer-controlled single-crystalline graphene film with stacking order via Cu−Si alloy formation. *Nat. Nanotechnol.* **2020**, *15* (10), 861−867.

(14) Wu, M.; Zhang, Z.; Xu, X.; Zhang, Z.; Duan, Y.; Dong, J.; Qiao, R.; You, S.; Wang, L.; Qi, J.; et al. Seeded growth of large single-crystal copper foils with high-index facets. *Nature* **2020**, *581* (7809), 406−410.

(15) Malard, L. M.; Pimenta, M. A.; Dresselhaus, G.; Dresselhaus, M. S. Raman spectroscopy in graphene. *Phys. Rep.* **2009**, *473* (5), 51−87.

(16) Casiraghi, C. Raman intensity of graphene. *physica status solidi (b)* **2011**, *248* (11), 2593−2597.

(17) Piscanec, S.; Lazzeri, M.; Mauri, F.; Ferrari, A. C.; Robertson, J. Kohn anomalies and electron-phonon interactions in graphite. *Phys. Rev. Lett.* **2004**, *93* (18), No. 185503.

(18) Piscanec, S.; Lazzeri, M.; Robertson, J.; Ferrari, A. C.; Mauri, F. Optical phonons in carbon nanotubes: Kohn anomalies, Peierls distortions, and dynamic effects. *Phys. Rev. B* **2007**, *75* (3), No. 035427.

(19) Lazzeri, M.; Piscanec, S.; Mauri, F.; Ferrari, A. C.; Robertson, J. Phonon linewidths and electron-phonon coupling in graphite and nanotubes. *Phys. Rev. B* **2006**, *73* (15), No. 155426.
(20) Khomyakov, P. A.; Giovannetti, G.; Rusu, P. C.; Brocks, G.; van den Brink, J.; Kelly, P. J. First-principles study of the interaction and charge transfer between graphene and metals. *Phys. Rev. B* **2009**, *79* (19), No. 195425.
(21) Giubileo, F.; Di Bartolomeo, A. The role of contact resistance in graphene field-effect devices. *Prog. Surf. Sci.* **2017**, *92* (3), 143−175.
(22) Haas, G. A.; Thomas, R. E. Work function and secondary emission studies of various Cu crystal faces. *J. Appl. Phys.* **1977**, *48* (1), 86−93.
(23) Skriver, H. L.; Rosengaard, N. M. Surface energy and work function of elemental metals. *Phys. Rev. B* **1992**, *46* (11), 7157−7168.
(24) Kawano, H. Effective Work Functions of the Elements. *Prog. Surf. Sci.* **2022**, *97* (1), No. 100583.
(25) Li, D.; Yang, P. B, N, and Si Single-Doping at Graphene/Cu (111) Interfaces to Adjust Electrical Properties. *Langmuir* **2023**, *39* (26), 9172−9179.
(26) Lee, J. E.; Ahn, G.; Shim, J.; Lee, Y. S.; Ryu, S. Optical separation of mechanical strain from charge doping in graphene. *Nat. Commun.* **2012**, *3*, 1024.
(27) Du, X.; Skachko, I.; Barker, A.; Andrei, E. Y. Approaching ballistic transport in suspended graphene. *Nat. Nanotechnol.* **2008**, *3* (8), 491−495.
(28) Luo, D.; Wang, M.; Li, Y.; Kim, C.; Yu, K. M.; Kim, Y.; Han, H.; Biswal, M.; Huang, M.; Kwon, Y.; et al. Adlayer-Free Large-Area Single Crystal Graphene Grown on a Cu(111) Foil. *Adv. Mater.* **2019**, *31* (35), No. e1903615.
(29) Yi, D.; Luo, D.; Wang, Z.-J.; Dong, J.; Zhang, X.; Willinger, M.-G.; Ruoff, R. S.; Ding, F. What Drives Metal-Surface Step Bunching in Graphene Chemical Vapor Deposition? *Phys. Rev. Lett.* **2018**, *120* (24), No. 246101.
(30) Novoselov, K. S.; Geim, A. K.; Morozov, S. V.; Jiang, D.; Katsnelson, M. I.; Grigorieva, I. V.; Dubonos, S. V.; Firsov, A. A. Two-dimensional gas of massless Dirac fermions in graphene. *Nature* **2005**, *438* (7065), 197−200.
(31) Takahashi, T.; Tokailin, H.; Sagawa, T. Angle-resolved ultraviolet photoelectron spectroscopy of the unoccupied band structure of graphite. *Phys. Rev. B* **1985**, *32* (12), 8317−8324.
(32) Wang, M.; Huang, M.; Luo, D.; Li, Y.; Choe, M.; Seong, W. K.; Kim, M.; Jin, S.; Wang, M.; Chatterjee, S.; et al. Single-crystal, large-area, fold-free monolayer graphene. *Nature* **2021**, *596* (7873), 519−524.
(33) Xu, Z.; Buehler, M. J. Interface structure and mechanics between graphene and metal substrates: a first-principles study. *J. Phys.: Condens. Matter* **2010**, *22* (48), No. 485301.
(34) Tang, K.; Qi, W.; Wei, Y.; Ru, G.; Liu, W. High-Throughput Calculation of Interlayer van der Waals Forces Validated with Experimental Measurements. *Research (Wash D C)* **2022**, *2022*, No. 9765121.
(35) Lou, S.; Ma, X.; Wang, Z.; Wang, W.; Song, L.; Sun, X.; Ding, Y.; Yin, W. J.; Yang, W.; Tan, J.; et al. Interfacial Coupling Induced Discrete Orientation of Epitaxial Graphene on High-Index Cu Substrates. *Adv. Funct. Mater.* **2024**, *35* (9), No. 2415972.
(36) Wang, J.; Wang, S.-Q. Surface energy and work function of fcc and bcc crystals: Density functional study. *Surf. Sci.* **2014**, *630*, 216−224.
(37) Filleter, T.; McChesney, J. L.; Bostwick, A.; Rotenberg, E.; Emtsev, K. V.; Seyller, T.; Horn, K.; Bennewitz, R. Friction and Dissipation in Epitaxial Graphene Films. *Phys. Rev. Lett.* **2009**, *102* (8), No. 086102.
(38) Dong, Y. Effects of substrate roughness and electron−phonon coupling on thickness-dependent friction of graphene. *J. Phys. D: Appl. Phys.* **2014**, *47* (5), No. 055305.
(39) Holscher, H.; Ebeling, D.; Schwarz, U. D. Friction at atomic-scale surface steps: experiment and theory. *Phys. Rev. Lett.* **2008**, *101* (24), No. 246105.
(40) Steiner, P.; Gnecco, E.; Krok, F.; Budzioch, J.; Walczak, L.; Konior, J.; Szymonski, M.; Meyer, E. Atomic-scale friction on stepped surfaces of ionic crystals. *Phys. Rev. Lett.* **2011**, *106* (18), No. 186104.
(41) Dong, Y.; Wu, X.; Martini, A. Atomic roughness enhanced friction on hydrogenated graphene. *Nanotechnology* **2013**, *24* (37), No. 375701.

https://doi.org/10.1021/prechem.6c00002
Precis. Chem. XXXX, XXX, XXX−XXX